

## Research Article

# Development of Image Segmentation Methods for Intracranial Aneurysms

**Yuka Sen, Yi Qian, Alberto Avolio, and Michael Morgan**

*The Australian School of Advanced Medicine, Macquarie University, Sydney, NSW 2109, Australia*

Correspondence should be addressed to Yi Qian; [yi.qian@mq.edu.au](mailto:yi.qian@mq.edu.au)

Received 17 January 2013; Accepted 8 March 2013

Academic Editor: Peng Feng

Copyright © 2013 Yuka Sen et al. This is an open access article distributed under the Creative Commons Attribution License, which permits unrestricted use, distribution, and reproduction in any medium, provided the original work is properly cited.

Though providing vital means for the visualization, diagnosis, and quantification of decision-making processes for the treatment of vascular pathologies, vascular segmentation remains a process that continues to be marred by numerous challenges. In this study, we validate eight aneurysms via the use of two existing segmentation methods; the Region Growing Threshold and Chan-Vese model. These methods were evaluated by comparison of the results obtained with a manual segmentation performed. Based upon this validation study, we propose a new Threshold-Based Level Set (TLS) method in order to overcome the existing problems. With divergent methods of segmentation, we discovered that the volumes of the aneurysm models reached a maximum difference of 24%. The local artery anatomical shapes of the aneurysms were likewise found to significantly influence the results of these simulations. In contrast, however, the volume differences calculated via use of the TLS method remained at a relatively low figure, at only around 5%, thereby revealing the existence of inherent limitations in the application of cerebrovascular segmentation. The proposed TLS method holds the potential for utilisation in automatic aneurysm segmentation without the setting of a seed point or intensity threshold. This technique will further enable the segmentation of anatomically complex cerebrovascular shapes, thereby allowing for more accurate and efficient simulations of medical imagery.

## 1. Introduction

Specification of intracranial aneurysm morphology and hemodynamic analysis requires segmentation of vascular geometries from three-dimensional (3D) medical images, produced via CTA or MRA. Methods for such manipulations of medical images are directly linked to the accuracy of aneurysm model construction, particularly regarding the geometry of complex shapes and volumes. In most cases, this process involves extraction of the 2D image from CTA or MRA, followed by reconstruction of the 3D aneurysm surface model. As such, several approaches exist and are currently utilized in cerebrovascular segmentation. On one hand, the fuzzy-based approach has been adapted for detecting malformed and small vessels in MRA images [1], while region growing approaches are popular in medical image segmentation due to their simplicity and computational efficiency [2]. Major problems, however, include leakage when the boundary is blurred and sensitivity to seed position. Utilization of implicit active contour methods within the level set framework seems to be widespread in medical image

segmentation [3–5] as the method does not suffer from parameterization surface problems [6] and has the capability to handle complex geometries and topological changes [7, 8]. More recently, active contour methods have also appeared in the modeling of intracranial aneurysms and cerebrovascular segmentation [9, 10]. Law and Chung proposed a method based upon multirange filters and local variances to perform the segmentation of intracranial aneurysms on Phase Contrast Magnetic Resonance Angiography data [11]. Hernandez and Frangi have developed a segmentation method for intracranial aneurysms based on Geometric Active Regions (GAR), using CTA and 3D Rotational Angiography data [12], whilst several Geodesic Active Contours (GAC) based methods have since been adapted for segmentation of brain aneurysms from CTA data [13, 14]. These methods either require sufficient training sets or they are reliant on boundary information obtained from medical imaging. Furthermore, boundary-based active contour level set methods may easily leak when the target boundary is not clearly defined. Though Firouzian et al. proposed a Geodesic Active Contours based level set method which employs region information and

intensity, it requires a user-defined seed point in order to calculate intensity threshold [15].

Despite the availability of many image segmentation methods, with varying approaches and algorithms, there is no dominant method in terms of effectiveness, across all areas [16–18]. Our previous study indicated that the volume of the aneurysm models depends strongly on the different segmentation methods. The segmentation method likewise influences the local geometric shapes of the aneurysms [19]. Validation will thus become necessary, comparing segmentation methods and adjusting the parameters of these segmentation techniques in order to assure the quality of patient-specific cerebral-vascular hemodynamic analysis. Although a number of commercial software packages for segmentation are available in the market, there is a conspicuous lack of discussion of methodology and information regarding validation processes.

In this paper, the authors propose a new Threshold-Based Level Set method for cerebral aneurysms. This method is based on the Geodesic Active Contours model [20] and Chan-Vese model (CV) [21] integrating both region and boundary information to segment cerebral aneurysms through the use of a global threshold and gradient magnitude to form the speed function. The initial threshold is calculated from the Chan-Vese model and is then iteratively updated throughout the process of segmentation. Upon reaching the aneurysm boundary, the change in the threshold value will decrease because of the contrast between aneurysm and nonaneurysm intensities and the iteration will stop. The algorithm may then be implemented in an automatic or semiautomatic manner depending on the complexity of the aneurysm shape.

The results of 3D automatic aneurysm segmentations, from the Region Growing Threshold (RGT), the Chan-Vese model (CV), and the Threshold-Based Level Set (TLS), are compared to results obtained via manual segmentation, performed by an expert radiologist over eight data sets of CTA imagery. Evaluation was based on six validation metrics: volume difference (VD), Jaccard's measure (volume overlap metric, JM), false positive ratio (rpf), false negative ratio (rfn), Hausdorff distance (maximum surface distance, HD), and mean absolute surface distance (MASD). This study will also discuss the impact of parameter adjustments on segmentation results.

## 2. Methods

**2.1. Region Growing Threshold Connecting (RGT).** The Region Growing Threshold method starts with a seed(s), selected within the area of the object to be segmented. It requires two intensity values for the pixel of the object, a low threshold  $T_1$ , and high threshold  $T_2$  values. Neighboring pixels whose intensity values fall within this range are accepted and included in the region. When no more neighbor pixels are found that satisfy the criterion, the segmentation is considered to have been completed. The selection criterion is described by the following equation:

$$I(X) \in [X - T_1, X + T_2], \quad (1)$$

where  $T_1$  and  $T_2$  represent the low and high thresholds of the region intensities,  $I(X)$  represent the image, and  $X$  the position of the particular neighboring pixel being considered for inclusion in the region. Problems surrounding RGT include threshold selection and sensitivity to seed position [22].

**2.2. Chan-Vese Model (CV) [21].** The Chan-Vese model is based upon the Mumford-Shah functional [23]. The associated evolution PDE in the level set framework is

$$\begin{aligned} \frac{\partial \varphi}{\partial t} = |\nabla \varphi| \left[ \lambda_2 (I - \mu_{\text{out}})^2 - \lambda_1 (I - \mu_{\text{in}})^2 - \alpha \right. \\ \left. + \beta \operatorname{div} \left( \frac{\nabla \varphi}{|\nabla \varphi|} \right) \right], \end{aligned} \quad (2)$$

where  $\mu_{\text{in}}$  is the mean of the target object of intensity,  $\mu_{\text{out}}$  represents the mean of the background of intensity, and  $\lambda_1, \lambda_2, \alpha$ , and  $\beta$  are positive constants. The Chan-Vese model does not require a term related to the image gradient. Instead, region intensity information is utilized for the target objects of segmentation. This model has exhibited significant effectiveness in segmentation of images with blurred boundaries.

**2.3. Threshold-Based Level Set (TLS).** The Threshold-Based Level Set combines both the Geodesic Active Contour and the Chan-Vese model within the level set framework.

Under the level set scheme, the contour is seen to deform by the function;  $\partial \Gamma(t)/\partial t + F|\nabla \varphi| = 0$ , with an embedded surface  $\Gamma(t)$  represented as the zero level set of  $\varphi$  by  $\Gamma(t) = \{x, y \in R \mid \varphi(x, y, t) = 0\}$ .

$F$  represents a function for speed, which drives the  $\Gamma(t)$  surface evolution in the normal direction. It is clear that  $F$  exerts a direct impact upon the quality of medical image segmentation. The associated evolution PDE in the level set framework is represented as follows:

$$\frac{\partial \varphi}{\partial t} = |\nabla \varphi| \left( \alpha (I - T) + \beta \operatorname{div} \left( g \frac{\nabla \varphi}{|\nabla \varphi|} \right) \right), \quad (3)$$

where  $I$  represents the image to be segmented,  $T$  the intensity threshold,  $g$  is the image gradient,  $\kappa = \operatorname{div}(\nabla \varphi/|\nabla \varphi|)$  the curvature,  $\alpha$  the image propagation constant, and  $\beta$  represents the spatial modifier constant for the curvature  $\kappa$ .  $\alpha$  and  $\beta$  serve to weight the relative influence of each of these terms on the movement of the surface contour.

The first term of the RHS of the formula,  $\alpha(I - T)$ , defines the region where  $T$  is an automatically defined parameter indicating the lower boundary of the intensity level for the target object. In this work, the target aneurysm is always assumed to possess a relatively higher intensity level than its background. It can thus be seen that this first term forces the contours to enclose regions with intensity levels greater than  $T$ . When the contour lies within the aneurysm region,  $(I - T) \geq 0$ , it expands in the normal direction. When  $(I - T) < 0$ , the contour lies beyond the aneurysm region and thus shrinks with a negative speed. This process stops when the contours converge to the aneurysm boundary, with the

TABLE 1: Validation results of segmentation methods.

	Case 1	Case 2	Case 3	Case 4	Case 5	Case 6	Case 7	Case 8	Average
VD (%)									
GT	0	0	0	0	0	0	0	0	
TLS	1.55	4.69	4.48	0.46	2.92	0.12	3.55	2.27	2.51
RGT	7.65	4.47	8.86	1.37	5.52	6.09	3.21	10.90	6.01
CV	11.63	18.23	5.60	4.04	2.47	2.51	24.18	14.02	10.34
JM (%)									
GT	100	100	100	100	100	100	100	100	
TLS	91.87	89.66	88.57	93.25	91.64	92.35	91.55	93.79	91.59
RGT	90.12	88.24	87.02	93.00	91.39	90.90	94.27	89.58	90.57
CV	88.24	84.02	86.73	89.53	91.85	91.82	76.96	89.59	87.34
rfp (%)									
GT	0	0	0	0	0	0	0	0	
TLS	4.97	2.91	3.20	1.65	3.60	3.99	4.06	2.11	3.31
RGT	0.64	3.80	14.72	0.92	9.22	1.64	5.95	0.13	4.63
CV	11.84	18.02	13.26	5.38	4.60	5.54	28.75	11.62	12.38
rfn (%)									
GT	0	0	0	0	0	0	0	0	
TLS	3.57	3.25	1.51	5.21	1.40	3.97	4.73	4.23	3.48
RGT	9.26	8.40	0.17	6.15	0.18	7.61	0.12	10.30	5.27
CV	1.32	0.84	1.78	5.66	3.93	3.09	0.92	0.00	2.19
HD (pixel)									
GT	0	0	0	0	0	0	0	0	
TLS	0.51	0.65	0.68	1.17	0.79	1.89	0.65	0.79	0.89
RGT	0.77	0.64	0.89	1.41	0.55	1.86	0.49	0.76	0.92
CV	0.75	1.17	1.04	2.09	1.19	0.51	1.00	0.95	1.09
MASD (pixel)									
GT	0	0	0	0	0	0	0	0	
TLS	0.08	0.08	0.07	0.09	0.07	0.05	0.07	0.10	0.08
RGT	0.10	0.10	0.12	0.10	0.10	0.07	0.07	0.10	0.10
CV	0.06	0.06	0.07	0.11	0.08	0.05	0.07	0.10	0.08

image  $I$  reaching a threshold of  $T$ . If we isolate this first term of the RHS of (3), it becomes the selection criteria for the lower threshold in the Region Growing Threshold method. The second term in the formula would likewise become the Geodesic Active Contour term.

**2.3.1. Method for Automatic Threshold Selection.** The Threshold-Based Level Set requires an appropriate estimate of the threshold value from proper segmentation of the aneurysm, obtained using Chan-Vese model and the statistical data specifically, confidence interval (CI) and confidence level (CL).

**2.3.2. Confidence Interval (CI) and Confidence Level (CL).** The confidence level (CL) represents how often the true percentage of a population lies within the confidence interval (CI). Based on Chebyshev's inequality [24] a general relationship for symmetric distribution between CI and CL can be established. The inequality for symmetric distribution is given as

$$P(|X - \mu| \geq k\sigma) \leq \frac{1}{k^2} \quad k > 0, \quad (4)$$

where  $X$  is the random variable population,  $\mu$  is the population mean, and confidence interval is represented by  $k$  times  $\sigma$  standard deviation. Equation (4) indicates that more than  $(1 - (1/k^2) \times 100)$  percent of the population lies between  $k$  standard deviations from the population mean.

For nonsymmetric distribution, the one-tailed version of the inequality is used. This is given by

$$P(X - \mu \geq k\sigma) \leq \frac{1}{1 + k^2} \quad k > 0. \quad (5)$$

For this inequality, it follows that when  $k = 1$ , more than 50% of the population is located one standard deviation away from the mean.

**2.3.3. Initial Threshold Selection.** According to the theory of confidence interval, the lower bound threshold of the aneurysm can be defined by

$$T_i = \mu_a - k_i \sigma_a \quad i \geq 0. \quad (6)$$

The threshold  $T$  represents the difference between the mean of the intensity of the aneurysm ( $\mu_a$ ) and  $k$  times its standard

deviation ( $\sigma_a$ ). The intensities of the aneurysm and its background regions are different, with the lowest intensity threshold of the aneurysm being the same as the highest intensity threshold of the background. Thus, the relationship  $\mu_b + k_b\sigma_b = \mu_a - k_a\sigma_a$  would apply. The confidence levels for both the aneurysm and its background are considered to be the same;  $k_b = k_a = k$ , thereby allowing  $k$  to be expressed as

$$k = \frac{\mu_a - \mu_b}{\sigma_a - \sigma_b}. \quad (7)$$

We have utilized the Chan-Vese model method to perform an initial segmentation. From the results obtained, the initial  $k_0$  was seen to be calculated via (7). The initial  $T_0$  can likewise be found using (6).

**2.4. Data Acquisition.** Clinical studies were performed with the consent of the patient in relation to acquisition of aneurysm images. These protocols were approved by the local institutional review board and the regional research ethics committee, with eight data sets of patients harboring internal carotid artery aneurysms acquired by 3D CTA scans (GE Healthcare).

Cross-sectional images were acquired by a CT angiography scanner with multidetector-row capability, a table speed of 9 mm/s, and zero-degree table (and gantry tilt). Scanning was initiated from the common carotid artery and continued parallel to the orbitomeatal line to the level of the Circle of Willis, during this intravenous injection of contrast material was administered at a rate of 3.5 mls/s. Aneurysm image was  $512 \times 512$  pixel field, while slices of continuous thickness were used to segment and reconstruct 3D vascular geometry. Pixels are expressed in Hounsfield Units (HU).

**2.5. Experiment Setting.** For quantitative evaluation, manual segmentation of eight aneurysms using open source software, 3D Slicer, was conducted by an expert radiologist. The results were utilized as a ground truth (GT) for the comparison of other methods. A region of interest (ROI), a good representation of the targeted region for segmentation, was selected depending on the aneurysm size. All the experiments were performed on cropped data sets to reduce calculation time and memory usage, with preparatory work being completed prior to the conduction of the experiments.

### 2.5.1. Parameter Setting

**The Threshold-Based Level Set.** The initial zero level set is a rectangular prism surface, constructed by the subtraction of two pixels on either side of the ROI. Thus, three parameters needed to be set:  $\alpha$ ,  $\beta$  from (3) and  $c$  from (8). All eight experiments utilized a fixed setting of  $\alpha = 10$ ,  $\beta = 3$ , and  $c$  in the range between 0.1 and 0.01. The role of this will be analyzed in Section 4.

**The Chan-Vese Model.** The initial zero level set is a cuboid surface, constructed in the same manner as the TLS, with the parameters in (2) fixed for all cases;  $\lambda_1 = \lambda_2 = 0.001$ ,  $\alpha = 0$ , and  $\beta = 0.3$ .

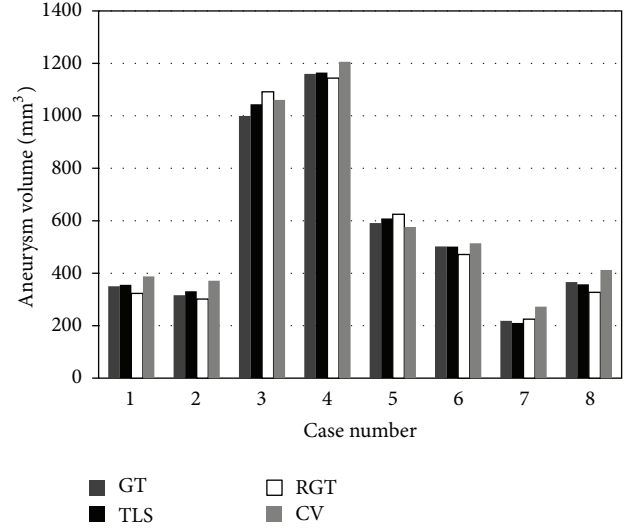


FIGURE 1: Aneurysm volume against segmentation methods.

**The Region Growing Threshold.** According to each case, an initial seed point is required to determine the starting loci within the specific aneurysm. For low and high intensity thresholds  $T_1$  and  $T_2$  in (1),  $T_1$  was selected to utilize the threshold of the TLS result for each case, with  $T_2$  representing the highest intensity of the aneurysm.

### 2.6. Evaluation

- (i) Aneurysm volume was calculated through the use of the boundary geometry, segmented using various methods. The volume difference (VD) was calculated using the equation  $VD = |(V_2 - V_1)/V_1| \times 100\%$ , where  $V_1$  represents the volume of GT and  $V_2$  represents the volume of the TLS, RGT, or CV methods.
- (ii) Jaccard's measure (JM) is a volume overlap metric, used to count the percentage of voxel intersections for the paired segmentations.

This can be seen as  $JM = 2 * |S_1 \cap S_2| / |S_1 \cup S_2|$ , where  $S_1$  represents the voxels created by the GT and  $S_2$  the voxels generated through the use of the TLS, RGT, or CV methods.

- (iii) False positive ratio (rpf) represents the percentage of the extra voxels of  $S_2$ , located outside of  $S_1$ . When the rpf equates to zero, no voxels in  $S_2$  will be located outside of  $S_1$ . Accordingly,  $rpf = (|s_2| - |s_1 \cap s_2|) / |s_1|$ , where  $S_1$  represents the voxels created by the GT and  $S_2$  represents the voxels generated by the TLS, RGT, or CV methods.
- (iv) False negative ratio (rfn) represents the percentage of the lost voxels of  $S_2$ , which cover the internal surface of the  $S_1$ .

This may be seen as  $rfn = (|s_1| - |s_1 \cap s_2|) / |s_1|$ , where  $S_1$  represents the voxels created by the GT and  $S_2$



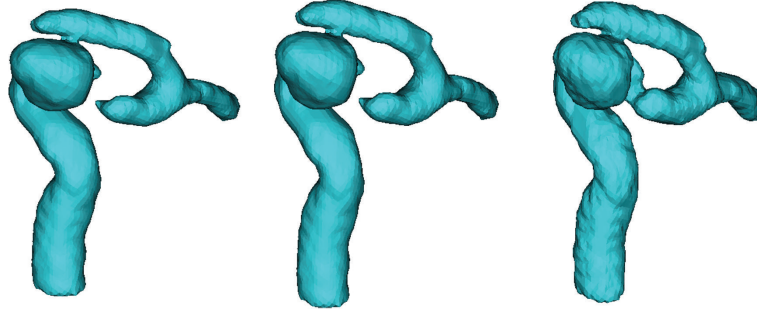


FIGURE 2: 3D geometries of segmentation results comparison, from left to right: CV, RGT, and TLS.



FIGURE 3: Segmentation results comparison (Case 1, aneurysm with bleb), from left to right: GT, CV, RGT, TLS, and photo from open head surgery.

represents the voxels generated by the TLS, RGT, or CV methods.

- (v) Hausdorff distance (HD) measures the maximum surface distance. This measure is extremely sensitive to outliers and may not reflect the overall degree of correlation.
- (vi) The mean absolute surface distance (MASD) indicates the average degree of difference between two surfaces and does not depend on aneurysm size [15].

### 3. Results

The calculated values of VD, JM, rfp, rfn, HD, and MASD for the eight cases considered are tabulated in Table 1. The average values are also shown. Figure 1 depicts the volume of the aneurysm. The minimum VD can be seen in the TLS method. The average value of VD is seen to be 2.51%. The maximum VD, however, is seen for Case 7 using the CV method. The values of JM indicate that the TLS method has the highest overlap rate in comparison to the other two methods, with an average of 91.59%. A study of rfp and rfn indicates a 3.31% overflow and 3.48% absence on average for the TLS method. The largest rfp and the smallest rfn were found to occur via the use of the CV method. These results likewise indicate that the largest volume was generated by the CV method, when compared to all other methods.

Results obtained for the surface distance metrics (HD and MASD) indicate the reliability of all segmentation methods, with the HD values for the TLS method being between 0.51 to 1.89 pixels and the maximum MASD being 0.08.

Figure 2 shows the 3D geometry of Case 4, restructured via three segmentation methods. Only TLS was effective in

fully reconstructing the parent artery and aneurysm, while the other two methods were not able to construct a portion of the artery. One reason for this is that the aneurysm size in Case 4 is larger in comparison to other cases. Another point is that the distal parent artery itself is curved to lie proximally to the aneurysm. These results likewise indicate that the TLS method may be utilized in the segmentation of aneurysms with blurred boundaries.

Figure 3 represents the segmented aneurysm surfaces of Case 1, where only TLS is able to restructure the bleb located at the top of the aneurysm. The resulting image is similar to the picture taken during open-skull surgery.

### 4. Discussion

**4.1. TLS Boundary Detect Function.** In this study, the TLS method utilizes a boundary feature map:

$$g(|\nabla I|) = \frac{1}{1 + c|\nabla I|^2}, \quad (8)$$

where  $g$  is for the detection of vascular boundaries,  $|\nabla I|$  represents a gradient magnitude, and  $c$  is a constant that controls the slope of the boundary detect function,  $g(|\nabla I|)$ . At the region of the artery and aneurysm, the boundary intensity gradient was seen to increase significantly. Thus, a relatively low  $c$  value was sufficient for the adjustment of the decreasing speed of  $g$ , in order to ensure that the search for the boundary surface was stopped at the arterial boundary. Figure 4 shows the process of selection for the value of  $c$  in Case 1; the results indicating that both VD and JM converged to a constant and MASD ceased all fluctuation when  $c$  was taken to equate to 0.5.

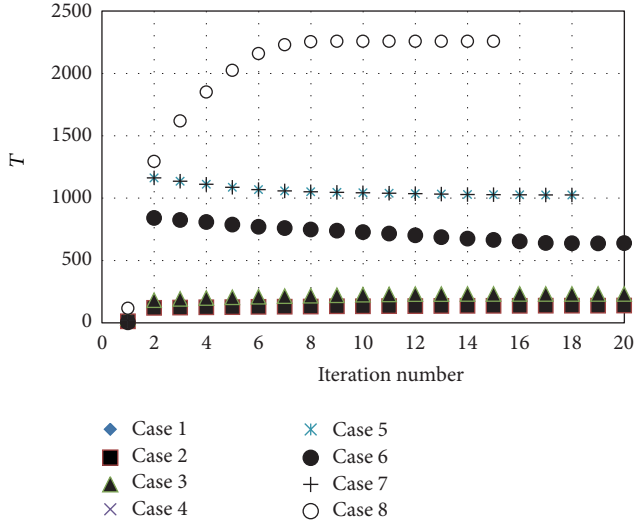


FIGURE 4: The convergence history of threshold  $T$ .

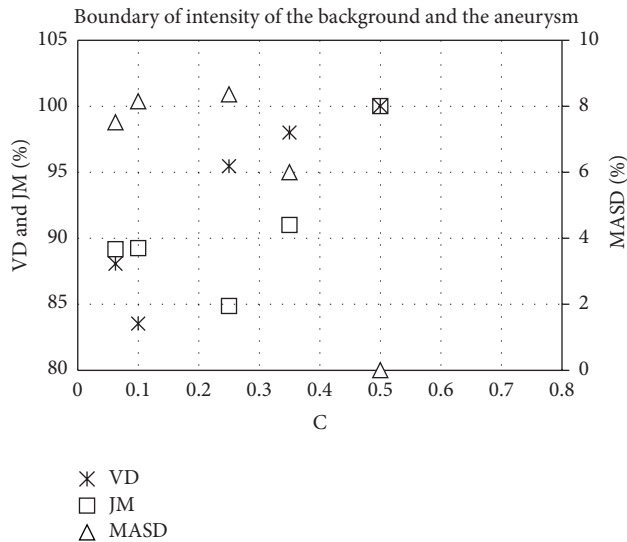


FIGURE 5: Validation of TLS boundary detect function  $C$  (Case 1).

**4.2. TLS Threshold.** The convergence history of threshold  $T$  is shown in Figure 5, with the  $T$  volumes exhibiting a tendency to converge after 15 iterations. The stability of the  $T$  volume against a range of value of  $c$  was likewise tested. The volume was found to be very stable for the range of  $c$  between 0.5 and 0.7. We thus suggest that the value of  $c$  is set at a volume between 0.5 and 0.7 for accurate boundary detection. As it is only TLS that does not require selection of any seeds during segmentation, it is suitable for the performance of automatic segmentations.

## 5. Conclusion

Various methods of segmentation generate a range of geometric models with changes in shape and volume, with the occurrence of uncertain results having the reductive

potential to negatively affect clinical treatment decisions. Through analysis of eight cerebral aneurysm models, this study indicated that limitations continue to surround current segmentation methods. The validation of the methods and analysis of errors seem vital. In this study, the TLS method was proposed to improve cerebrovascular aneurysm segmentation application. It is a technique with the ability to segment aneurysms anatomically without the setting of a seed point or intensity threshold. The method is also suitable for the segmentation of complex cerebrovascular anatomical shapes.

## Acknowledgments

The authors would like to thank members of Macquarie Medical Imaging, Macquarie University Hospital, for their kind support and contributions to these cases.

## References

- [1] N. D. Forkert, A. Schmidt-Richberg, J. Fiehler et al., "Fuzzy-based vascular structure enhancement in Time-of-Flight MRA images for improved segmentation," *Methods of Information in Medicine*, vol. 50, no. 1, pp. 74–83, 2011.
- [2] B. E. Chapman, J. O. Stapelton, and D. L. Parker, "Intracranial vessel segmentation from time-of-flight MRA using pre-processing of the MIP Z-buffer: accuracy of the ZBS algorithm," *Medical Image Analysis*, vol. 8, no. 2, pp. 113–126, 2004.
- [3] M. Droskey, B. Meyerz, M. Rumpfy, and K. Schaller, "An adaptive level set method for medical image segmentation," in *Proceedings of the Annual Symposium on Information Processing in Medical Imaging*, London, UK, 2001.
- [4] M. E. Leventon, W. E. L. Grimson, and O. Faugeras, "Statistical shape influence in geodesic active contours," in *Proceedings of IEEE Conference on Computer Vision and Pattern Recognition (CVPR '00)*, pp. 316–323, June 2000.
- [5] P. A. Yushkevich, J. Piven, H. C. Hazlett et al., "User-guided 3D active contour segmentation of anatomical structures: significantly improved efficiency and reliability," *NeuroImage*, vol. 31, no. 3, pp. 1116–1128, 2006.
- [6] J. A. Sethian, *Level Set Methods and Fast Marching Methods: Evolving Interfaces in Geometry, Fluid Mechanics, Computer Vision, and Materials Science*, Cambridge University, 2nd edition, 1999.
- [7] M. Kass, A. Witkin, and D. Terzopoulos, "Snakes: active contour models," *International Journal of Computer Vision*, vol. 1, no. 4, pp. 321–331, 1988.
- [8] S. Osher and J. A. Sethian, "Fronts propagating with curvature-dependent speed: algorithms based on Hamilton-Jacobi formulations," *Journal of Computational Physics*, vol. 79, no. 1, pp. 12–49, 1988.
- [9] S. Demirci, G. Lejeune, and N. Navab, "Hybrid deformable model for aneurysm segmentation," in *Proceedings of IEEE International Symposium on Biomedical Imaging: From Nano to Macro (ISBI '09)*, pp. 33–36, July 2009.
- [10] N. Wilson, K. Wang, R. W. Dutton, and C. Taylor, "A software framework for creating patient specific geometric models from medical imaging data for simulation based medical planning of vascular surgery," in *Proceedings of the 4th International Conference on Medical Image Computing and Computer-Assisted Intervention (MICCAI '01)*, pp. 449–456, 2001.

- [11] M. W. K. Law and A. C. S. Chung, "Vessel and intracranial aneurysm segmentation using multi-range filters and local variances," in *Proceedings of the International Conference on Medical Image Computing and Computer-Assisted Intervention (MICCAI '07)*, vol. 10, part 1, pp. 866–874, 2007.
- [12] M. Hernandez and A. F. Frangi, "Non-parametric geodesic active regions: method and evaluation for cerebral aneurysms segmentation in 3DRA and CTA," *Medical Image Analysis*, vol. 11, no. 3, pp. 224–241, 2007.
- [13] T. Deschamps, P. Schwartz, D. Trebotich, P. Colella, D. Saloner, and R. Malladi, "Vessel segmentation and blood flow simulation using level-sets and embedded boundary methods," *International Congress Series*, vol. 1268, pp. 75–80, 2004.
- [14] R. Manniesing, B. K. Velthuis, M. S. van Leeuwen, I. C. van der Schaaf, P. J. van Laar, and W. J. Niessen, "Level set based cerebral vasculature segmentation and diameter quantification in CT angiography," *Medical Image Analysis*, vol. 10, no. 2, pp. 200–214, 2006.
- [15] A. Firouzian, R. Manniesing, Z. H. Flach et al., "Intracranial aneurysm segmentation in 3D CT angiography: method and quantitative validation with and without prior noise filtering," *European Journal of Radiology*, vol. 79, no. 2, pp. 299–304, 2011.
- [16] T. Zuva, O. O. Olugbara, S. O. Ojo, and S. M. Ngwira, "Image segmentation, available techniques, developments and open issues," *Canadian Journal on Image Processing and Computer Vision*, vol. 2, no. 3, pp. 20–29, 2011.
- [17] H. Zhang, J. E. Fritts, and S. A. Goldman, "Image segmentation evaluation: a survey of unsupervised methods," *Computer Vision and Image Understanding*, vol. 110, no. 2, pp. 260–280, 2008.
- [18] D. Lesage, E. D. Angelini, I. Bloch, and G. Funka-Lea, "A review of 3D vessel lumen segmentation techniques: models, features and extraction schemes," *Medical Image Analysis*, vol. 13, no. 6, pp. 819–845, 2009.
- [19] Y. Sen, Y. Qian, Y. Zhang, and M. Morgan, "A comparison of medical image segmentation methods for cerebral aneurysm computational hemodynamics," in *Proceedings of the 4th International Conference on Biomedical Engineering and Informatics (BMEI '11)*, vol. 2, pp. 901–904, 2011.
- [20] V. Caselles, R. Kimmel, and G. Sapiro, "Geodesic active contours," *International Journal of Computer Vision*, vol. 22, no. 1, pp. 61–79, 1997.
- [21] T. F. Chan and L. A. Vese, "Active contours without edges," *IEEE Transactions on Image Processing*, vol. 10, no. 2, pp. 266–277, 2001.
- [22] Hu, Grossberg, and Mageras, "Survey of recent volumetric medical image segmentation techniques," in *Biomedical Engineering*, C. A. B. de Mello, Ed., InTech, 2009.
- [23] D. B. Mumford and J. Shah, "Optimal approximations by piecewise smooth functions and associated variational problems," *Communications on Pure and Applied Mathematics*, vol. 42, no. 5, pp. 577–685, 1989.
- [24] J. Russell and R. Cohn, *Chebyshev's Inequality*, Book on Demand, 2012.